

Regional Wave Propagation in and around the Tibetan Plateau

T.J. Owens, H.P. Crotwell, D.E. McNamara‡, G.E. Randall†

Department of Geological Sciences
University of South Carolina
Columbia, SC 29208

AFOSR Contract No. F49620-94-1-0066

and

AFOSR AASERT Contract No. F49620-94-1-0271

ABSTRACT

The Tibetan Plateau is a dominant structural feature influencing seismic wave propagation in Central Asia. Using data from the 1991-92 Tibetan Plateau Seismic Experiment deployment of broadband PASSCAL sensors, we are studying the effects of the Tibetan Plateau on a variety of regional phases propagating within the plateau and crossing its boundaries. In this report, we summarize results from two such studies. First, the propagation and attenuation characteristics of Lg are used to document that Lg can propagate within the thickened crust of the Tibetan Plateau and to confirm previous studies showing that all boundaries of the plateau are effective barriers to Lg propagation. Our results further indicate that attenuation of Lg within the plateau is relatively high, comparable to areas of active tectonics, such as the Basin and Range Province. The second study involves waveform modeling of Pn and Sn waveforms from regional events of moderate magnitude. Source mechanisms for these events have been recently published, providing the necessary constraints to begin detailed structural modeling. It has been known for a decade that there are significant lateral variations in Sn propagation within the plateau, specifically that the central northern Tibetan Plateau blocks the propagation of high-frequency Sn phases. Using broadband regional seismograms from events within the plateau, we document that this blockage is strongly frequency-dependent. The available station spacing allows us to observe a rapid loss of high frequencies as regional S phases cross into the northern plateau while frequencies below 0.05Hz propagate throughout the plateau. Variations in the displacement pulse-shapes through the transition into the northern plateau are more easily explained by a changes in Poisson's ratio with depth than by simply rapid changes in the attenuation structure.

† Now at: Los Alamos National Laboratory

‡ Now at: Lawrence Livermore National Laboratory

Keywords: regional phase propagation, Tibetan Plateau, Lg , Pn , Sn

19960624 119

OBJECTIVE

One approach to calibrating areas of nonproliferation concern is the use of mobile arrays of new generation, high dynamic range, broadband digital seismic instruments. This project uses existing data from a variety of seismic deployments to assess the utility of this approach and to develop strategies for using temporary deployments to gather data relevant to seismic monitoring concerns. We focus on regional structure and wave propagation studies of importance to understanding wave propagation in Central Asia using a large scale lithospheric profile (The 1991-92 Tibetan Plateau Broadband Seismic Experiment). Another aspect of our contract, the characterization of lithospheric heterogeneities and their influence on regional wave propagation is addressed in an accompanying paper by Greg Wagner.

PRELIMINARY RESEARCH RESULTS

We review results from two related studies intended to better define the characteristics of regional phase propagation in and around the Tibetan Plateau. The first is a completed study of *Lg* propagation and attenuation (McNamara et al, 1995a) and the second is an ongoing study of the lateral variations in *Pn* and *Sn* propagation.

Lg Propagation within the Tibetan Plateau. The propagation of *Lg* has been observed across most of Asia and the Indian Shield, however, *Lg* has not been observed for paths crossing through the Tibetan Plateau (e.g. Ruzaiкин et al., 1977; Ni and Barazangi, 1983). This effect has been attributed to either scattering due to a change in the crustal thickness and/or structural discontinuities at the boundaries of the plateau or an unusual velocity structure or high attenuation within the plateau. Previous studies were limited since they had to rely on stations outside of the Tibetan Plateau. They were only able to observe *Lg* for paths that cross the boundaries of the plateau. Consequently, they were not able to distinguish between the effects that the interior of the plateau versus its boundaries may have on *Lg* amplitudes.

We study the nature of *Lg* propagation and attenuation in two parts. First, we attempt to qualitatively analyze *Lg* attenuation and blockage by visually inspecting *Lg* amplitudes for paths crossing through the Tibetan Plateau and surrounding regions (Figure 1). Second, we invert *Lg* amplitudes, from paths restricted to the Tibetan Plateau, for frequency dependent attenuation (Figure 2).

The most significant new observations from our dataset is that *Lg* propagates within the Tibetan Plateau and that both the northern and southern boundaries of the plateau effectively block *Lg* propagation. We have observed strong *Lg* at every station from events with epicenters within the plateau. Though *Lg* is generated on the plateau, for our data set ($M_b=3.7-5.5$), we find that energy is quickly attenuated for event/station paths within the plateau that are greater than about 600-700 km. Events to the north of the Tibetan Plateau do not have observable *Lg* energy at recording stations within the Tibetan Plateau. This suggests that the northern boundary of the plateau blocks *Lg* transmission. We do, however, observe *Lg* at our stations at the northern edge of the plateau for long paths (> 700 km) from these same events north of the plateau, suggesting that the Tarim and Qaidam Basins allow for more efficient propagation of *Lg* than the Tibetan Plateau. We also confirm previous observations that the southern boundary of the Tibetan Plateau blocks *Lg* propagation (Ruzaiкин et al., 1977; Ni and Barazangi, 1983).

In order to quantify our inferred high attenuation, we have examined the amplitudes of *Lg* arrivals from events within the Tibetan Plateau for apparent Q . This may provide information to compare our observed *Lg* propagation to other regions throughout the world. Details of this analysis can be found in McNamara et al (1995a).

The inversion was performed over five octaves with center frequencies of 0.75, 1.5, 3, 6 and 12 Hz. Figure 2a shows *Lg* amplitude data with the source and receiver contributions removed. As is often observed, Q increases with increasing frequency. However, our measured Q for the Tibetan Plateau is low relative to other continental regions (Benz et al., 1994). A least squares fit to the plateau data is shown in Figure 2b and gives:

$$Q(f) = (279 \pm 39.5)f^{(0.53 \pm 0.09)} \quad (0.5 \leq f \leq 16\text{Hz}).$$

Using Figure 2b, it is possible to compare our value of $Lg Q(f)$ with other tectonic regions. The highest values for Q_0 are for stable continental paths. Low Q values are generally observed in tectonically active regions. Comparison of our results with regions in North America suggest that $Lg Q_0$ within the Tibetan Plateau is well below the eastern and central US and only slightly above the Basin and Range values. This suggests that the Tibetan Plateau is more similar to a tectonically active region than a stable continental interior or passive margin. However, a complicating factor in making these comparisons is the role of the thickened crust in the Tibetan Plateau in the development and propagation of Lg . If the thickened crust leads to an increase in the thickness of the Lg waveguide, then the intrinsic Q of the plateau could be higher while the Q estimated from Lg would remain low due to the energy lost in a thickened waveguide. Additional analysis is needed to understand this potential trade-off.

Lateral Variations in Sn Propagation in the Tibetan Plateau. It has been known since the early 1980's from the work of Ni and Barazangi that high-frequency Sn waves do not propagate across the northern Tibetan Plateau. We use broadband regional seismograms recorded during the 1991-92 Tibetan Plateau Seismic Experiment to analyze this phenomena over a much broader frequency band. The long-range goal of this study is to identify one or more causal mechanisms for the observed propagation effect and to constrain the physical state of the upper mantle beneath the Tibetan Plateau.

Spectral and spatial variations in regional S-wave propagation within the Tibetan Plateau were analyzed using highpass filtered, regional, broadband displacement seismograms. Then, these seismograms from regional events were examined to uncover variations in waveforms of Pn and Sn that might be related to the anomalous region. Lastly, we calculated complete regional synthetic seismograms using the reflectivity method to examine the effects of velocity gradients and attenuation on Pn and Sn waveforms.

High pass filters were applied to the regional data set with corners at 1, 0.2, 0.1, and 0.02 Hz. For each station event pair, we calculated the $Pcoda$ to Sn amplitude ratio using filtered displacement seismograms. The Sn amplitudes were measured for a window around the expected Sn arrival time on the tangential component while the $Pcoda$ amplitudes were measured for a window before the Sn arrival on the vertical component. $Pcoda$ amplitudes were measured in the vertical component due to its relatively small dependence on source mechanism while the Sn amplitudes were measured in the tangential component because this was generally the strongest arrival. $Pcoda$ to Sn ratios below 1.0 indicate that Sn is clearly visible while $Pcoda$ to Sn ratios greater than 2.0 indicate that Sn is absent. Many intermediate values were obtained, but we display the end-members since they most clearly illustrate the spatial and frequency dependence of the data.

When the results of this analysis are summarized by plotting each ray path with a line intensity indexed to the $Pcoda$ to Sn ratio, the spatial and spectral variation becomes clear (Figure 3). For frequencies above 1 Hz, there is a clearly defined region of inefficient Sn propagation in the northern plateau. We found it to be somewhat larger than the region defined by Ni and Barazangi (McNamara et al, 1995b). However, as longer period Sn energy is included in the ratio measure, Sn propagates in an increasingly larger portion of the plateau. At the longest periods measured, Sn propagates efficiently throughout the entire plateau.

In addition to the spectral and spatial variation, there are other observations that can be seen from this analysis. First, Sn is attenuated over distances of less than 200 kilometers as it enters the northern plateau. There are several conveniently located events that show clear Sn energy at stations just outside of the zone of inefficient Sn propagation and little to no Sn energy at nearby stations just inside of the zone. Secondly, the longest regional paths for events located in the far western plateau occasionally have visible S-wave energy after passing through the anomalous zone. Since these paths are nearly 20° long, the energy is unlikely to be Sn . However, it does suggest that there is a depth limit to the zone that attenuates S-waves.

Figure 4 displays several views of broadband displacement seismograms for event 92.095.17.42.50 (see inset for location). Paths for this event propagate nearly parallel to our network, thus eliminating the need to consider source mechanism in these displays. The path to AMDO does not enter the northern plateau anomalous zone, while the paths to WNDO, ERDO, and BUDO represent increasing path lengths within the zone. There are only minor variations in the P_n waveforms along the line (Figure 4). However, there are significant variations in S_n waveforms (Figure 4). For example, there is a dramatic change in frequency content between AMDO and WNDO that marks the boundary of the anomalous region. In Figure 4, the traces for S_n waveforms and P_n waveforms for the same station-event pair are displayed. Amplitudes are normalized for each trace to allow easy comparisons. Note the change in waveform shape as S_n propagates into the northern plateau. At AMDO (top left), the P_n and S_n waveforms are similar in shape. The S_n waveform begins to broaden at WNDO and has become significantly wider than the P_n waveform at ERDO, within the anomalous zone. At BUDO, the S_n waveform is essentially a broad step, significantly different from the more pulse-like P_n waveform. This difference is consistent with the loss of high-frequency S_n within this region.

Complete reflectivity modeling was used to compare the effects of attenuation and gradients on the shape of waveforms (Randall, 1994; Kennett, 1983). In our simplified modeling efforts, we did not attempt to compute seismograms for specific source mechanisms, but rather, we used the vertical component of the Green's function for the moment tensor source M_{xx} for P_n and the tangential component for S_n . The M_{xx} source is chosen purely for illustrative purposes and is clearly not physically reasonable. Also, source depth and crustal thickness are not intended to be realistic for the Tibetan Plateau. The modeling is only intended to explore the sensitivity of P_n and S_n waveforms to upper mantle velocity parameters. Comparisons between the Q models and the negative velocity gradient models are emphasized because these models show characteristics that are consistent with our observations. The positive velocity gradients show nearly constant pulse-like P_n and S_n waveforms. In addition, McNamara et al (1995b) found little evidence for positive velocity gradients in the regional P-wave data.

To begin to analyze the unusual waveform variations in our data, we used the reflectivity method to generate synthetic seismograms for three simple models. In each case a constant velocity crust with a thickness of 40 kilometers exists above the upper mantle. Within this upper mantle a velocity gradient exists for the upper 60 kilometers and a constant velocity half space exists below that. All variations in velocity and Q occurred in this upper mantle layer. The velocity models are radially symmetric, and so an earth-flattening transformation is applied before the reflectivity synthetics are calculated.

The first type of model was a positive velocity gradient below the Moho. The range of gradients was from .001 to .004 km/s/km in P-wave velocity. Poisson's ratio was held constant throughout the model. The second type of model was a negative velocity gradients below the Moho. The range in gradients is from -0.001 to -0.004 km/s/km in P-wave velocity and again, Poisson's ratio was held constant throughout the model. The third type of model was a variable Q structure within the upper mantle. In this case, no velocity gradients were used. A constant Q_p to Q_s ratio of 2 was assumed with Q_p values of 2000, 1000, 500, 250 and 124.

Analysis of the maximum envelope of negative gradients and Q_s with distance showed that, in general, negative velocity gradient models show faster amplitude decays with distance than the Q models tested. In addition, there is little variation in the decay curves for P_n and S_n phases. In order to observe the frequency variation, we looked at the waveshape variation for the negative gradient and Q models (Figure 5). Two critical observations were made here. First, negative gradient models always produce a broader, more step-like waveshape than do the Q models. Second, the S_n and P_n waveshapes are similar whether Q or the gradient is being varied. Our modeling to date is clearly preliminary. However, the results show considerable promise and allow some speculation as to the cause of the anomalous S_n zone. We have observed that S_n waveforms broaden quickly in the northern plateau and become step-like within a few hundred kilometers. However, P_n waveforms maintain a more pulse-like waveform within the northern plateau. Our modeling suggests that negative velocity gradients can most efficiently produce a step-like waveform. Very low Q structures can also produce step-like waveshapes, but would require long path lengths with seemingly unrealistic Q values. Finally, neither negative gradient models nor low Q models can produce different P_n and S_n waveshapes with constant $Q_p:Q_s$ and $V_p:V_s$ ratios.

Based on these results, we believe a defensible hypothesis for continuing analysis is that the S_n waveform distortion within the northern plateau is the result of a negative velocity gradient in the upper mantle. Since the P_n waveshape is not modified in this region, it is unlikely that a significant negative velocity gradient exists for P_n in the upper mantle. This would imply that Poisson's ratio varies in the upper mantle beneath the northern Tibetan Plateau. This variation may be the result of a high geothermal gradient and/or the existence of partial melt in the upper mantle. Similar phenomena has been suggested to explain differences in P_n and S_n seismograms at higher frequencies in other areas (Gajewski et al, 1990). Our continuing analysis involves waveform modeling of specific events to verify if the suggested phenomena can explain the observed lateral variations in S_n and P_n propagation in this region.

CONCLUSIONS AND RECOMMENDATIONS

Temporary broadband networks are clearly an advantage to efforts to calibrate relatively unknown regions. Our results demonstrate the type of information that can be determined with this type of data. Our L_g results have clarified a long-standing debate about the cause of L_g blockage by the Tibetan Plateau. Understanding the nature of this blockage is critical to understanding the effect it has on common discriminants that utilize L_g . Our preliminary calculations (McNamara et al, 1995a) indicate that P/L_g ratio discriminants would not be effective for events crossing a plateau boundary, but the existence of L_g within the plateau suggests that it may still be useful for certain paths. The unusual propagation characteristics of S_n also lead to anomalous waveforms that need to be understood before regional waveforms from this area can be confidently used for seismic monitoring measurements. In the future, we will continue to investigate the structure of the Tibetan Plateau utilizing this unique data set. The suggestion that a depth-varying Poisson's ratio is a reasonable mechanism for explaining our observed waveform behavior will be studied in detail as will the correlation of the anomalous S_n zone with a low P_n velocity region in the northern plateau. In addition, using the sources (Randall et al, 1995) and structural information derived in our work, we will be compiling common discriminant measurements for many regional events in the plateau to better document the influence the unusual regional structure may have on event discrimination in Central Asia.

REFERENCES

- Benz, H. M., R. Buland, and A. Frankel (1994). Source and structure studies using the U. S. national seismographic network (abstract), *Sixth annual IRIS workshop*, 7.
- Gajewski, D., R. Stangl, K. Fuchs, and K.J. Sandmeier, (1990). A new constraint on the composition of the topmost continental mantle-anomalous depth increases of P and S velocity, *Geophys. J. Int.*, 103, 497-507.
- Kennett, B.L.N. (1983). *Seismic Wave Propagation in Stratified Media*, Cambridge University Press, Cambridge, England, 342 pages.
- McNamara, D. E., T. J. Owens, and W. R. Walter (1995a). Propagation characteristics of L_g across the Tibetan Plateau, *Bull. Seis. Soc. Am*, submitted 1995.
- McNamara, D. E., T. J. Owens, and W. R. Walter (1995b). Observations of regional phase propagation across the Tibetan Plateau, *J. Geophys. Res.*, in press.
- Ni, J. and M. Barazangi (1983). High frequency seismic wave propagation beneath the Indian shield, Himalayan arc, Tibetan Plateau and surrounding regions: high uppermost mantle velocities and efficient propagation beneath Tibet, *Geophys. J. R. Astr. Soc.*, 72, 665-689.
- Randall, G.E. (1994). Efficient calculation of complete differential seismograms for laterally homogeneous earth models, *Geophys. J. Int.*, 118, 245-254.
- Randall, G.E., C.J. Ammon, and T.J. Owens (1995). Moment-tensor estimation using regional seismograms from portable network deployments, *Geophys. Res. Lett.*, July 1 issue.
- Ruzaikin, A., I. Nersesov, V. Khalturin, and P. Molnar (1977). Propagation of L_g and lateral variations in crustal structure in Asia, *J. Geophys. Res.*, 82, 307-316.
- Please refer to McNamara et al (1995a) for a complete list of references for Figure 2b.

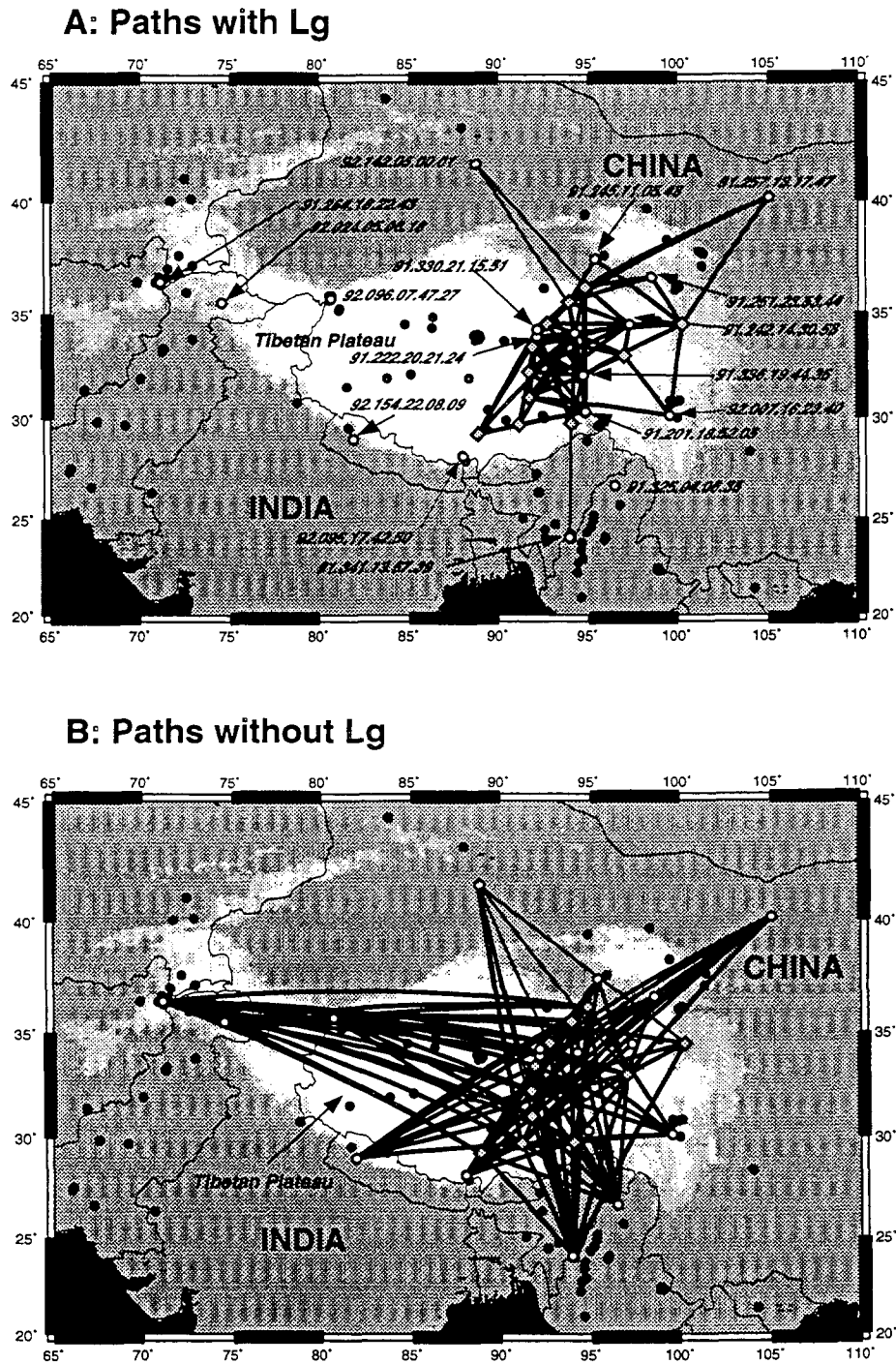


Figure 1. Representative paths showing the variation of Lg propagation within the Tibetan Plateau. Paths showing observable Lg (Top Frame) are restricted to paths in the eastern plateau, generally less than 700km in length. Paths without observable Lg (Bottom Frame) include those that cross the plateau boundaries and a few long paths from the western plateau.

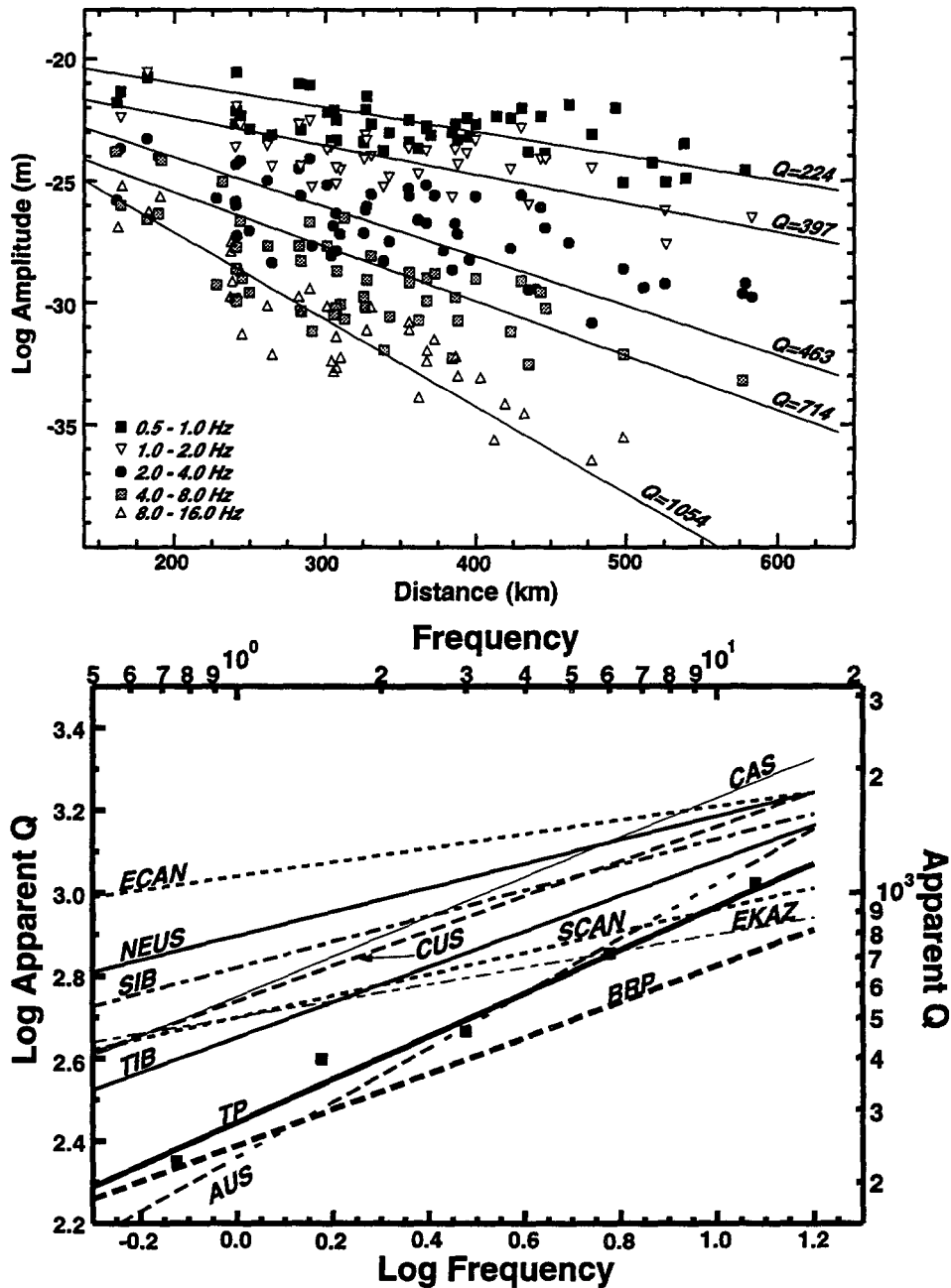


Figure 2. (Top) Lg amplitude versus distance for 5 octaves in frequency from 0.5 to 16 Hz. (Bottom) Apparent Q versus frequency for the Tibetan Plateau (Line Labeled TP) compared to worldwide observations including the northeastern United States (NEUS), central United States (CUS), Basin and Range province of North America (BRP) (Benz et al., 1994), Russian explosion recorded in central Asia (CAS) and stations in Siberia (SIB) (Xie, 1993), eastern Canada (ECAN) (Atkinson, 1989), eastern Kazakstan (EKAZ) (Sereno, 1990), Scandinavia (SCAN) (Sereno et al., 1988), Australia (AUS) (Bowman and Kennett, 1991), and a previously determined value for the Tibetan Plateau (TIB) (Shih et al., 1994). Axes are displayed as both frequency versus apparent Q and log frequency versus log apparent Q. $Q(f)$ was determined assuming a geometric spreading term of 0.5.

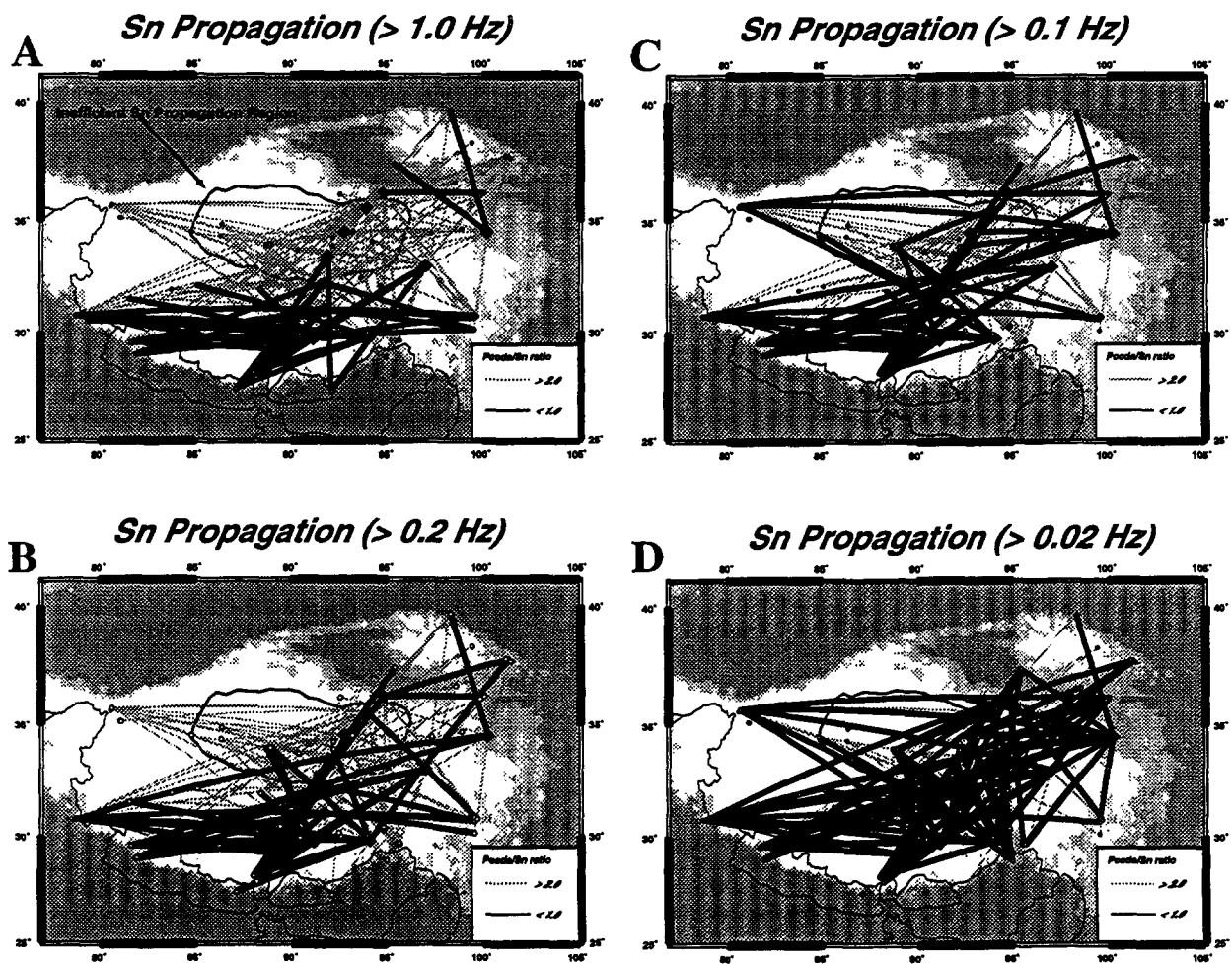
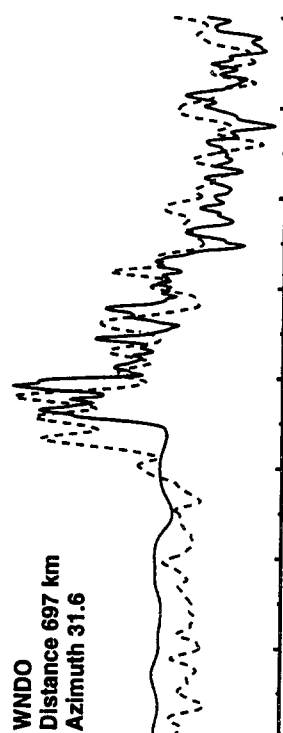


Figure 3. Four passbands illustrating the variation in Sn propagation efficiency spatially and with frequency. In each passband, the tangential Sn amplitude is compared to the P coda amplitude on the vertical component. This gives a stable measure of the "existence" of Sn energy in that passband. Gray colored paths indicate paths for which the P coda energy was more than twice the Sn energy. Black paths are where P coda energy is less than Sn energy. The region of the north-central plateau that is known to block high-frequency Sn is clearly visible in the higher frequencies, but disappears at longer periods.



**Pn and Sn Waveform Comparison for
Event 95.095.17.42.50**

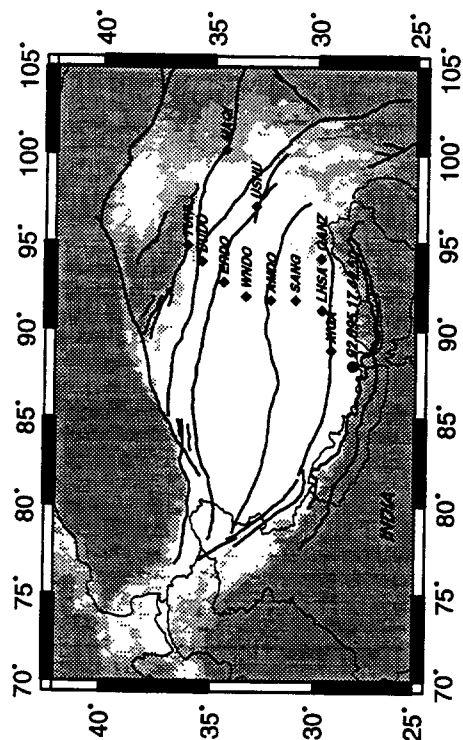
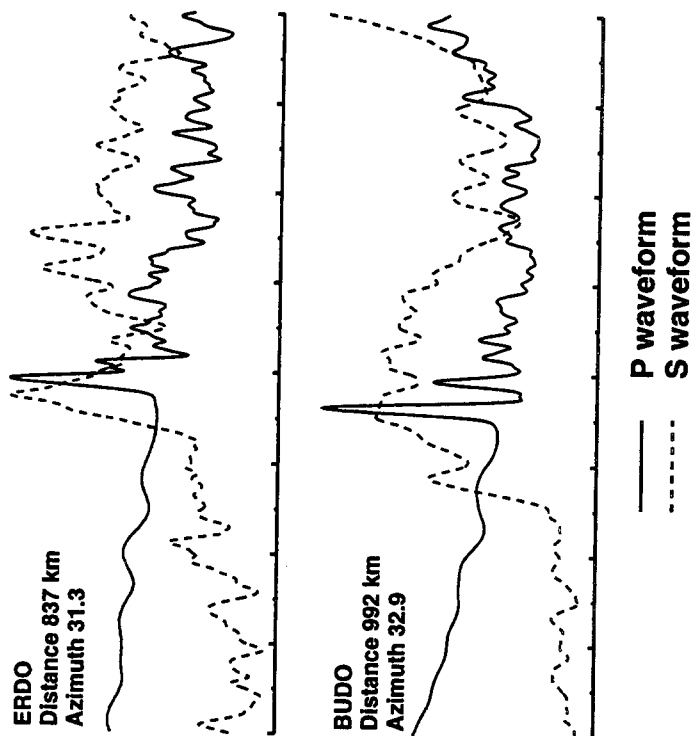


Figure 4. Variations in Pn and Sn waveforms across the Tibetan Plateau. Event 95.095.17.42.50 is located south of the network (see reference map), so energy propagates nearly in-line with the network. In each frame, the solid line is the Pn broadband displacement waveform and the dashed line is the Sn broadband displacement waveform. At AMDO, before the attenuating zone, the Pn and Sn waveforms are similar in shape. As the energy propagates to the north, the Pn waveform is relatively unchanged while the Sn waveform loses high frequencies and becomes a broad step in displacement.

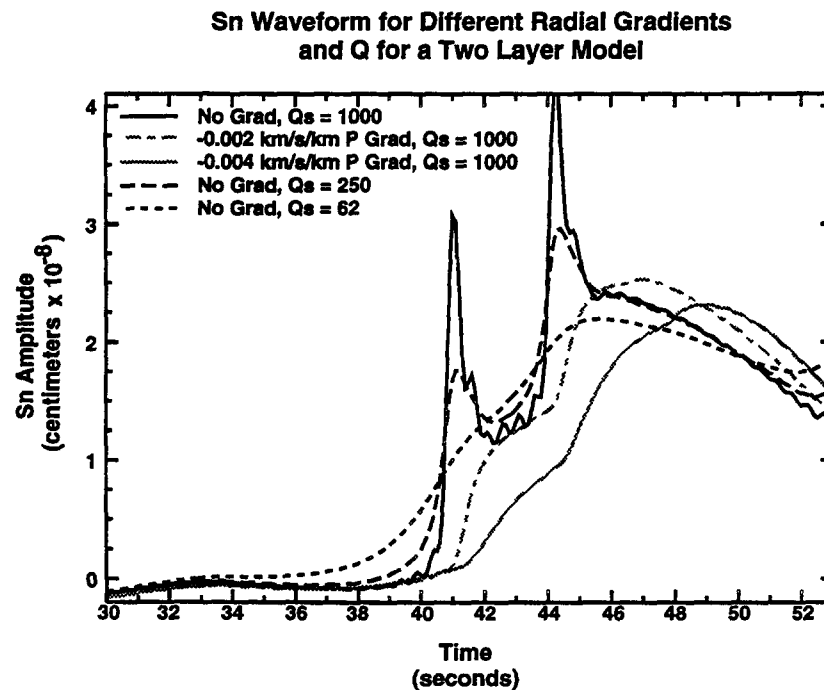
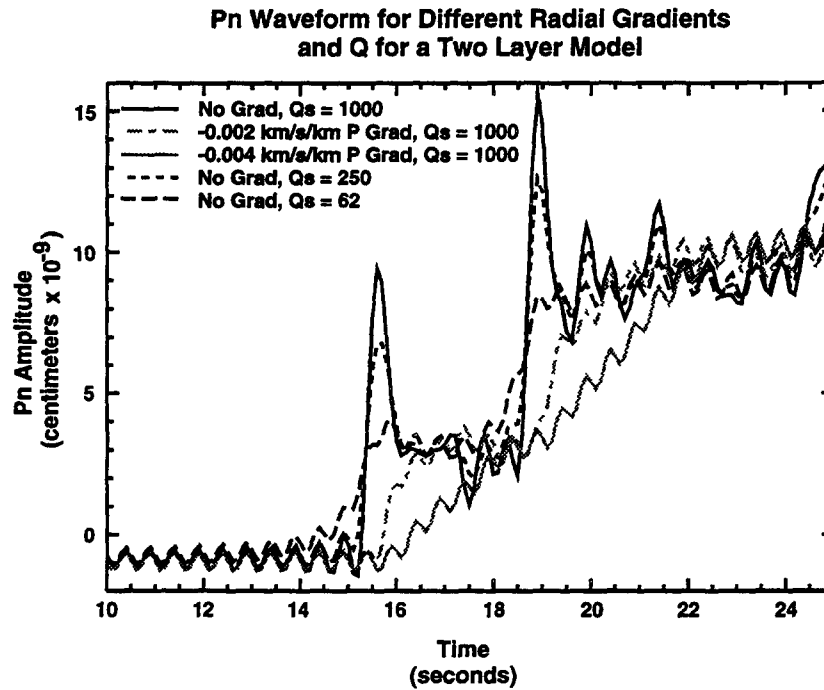


Figure 5. Synthetic analysis of the effects of negative velocity gradients and Q. Key in the upper left of each frame identifies the parameters of the models. The general observations are: 1) Sn and Pn waveshapes for a given model are roughly the same (this does not match the data), 2) Negative velocity gradients are more effective at broadening the Sn waveform than Q for reasonable values of each. A possible explanation is that the P-velocity and S-velocity may vary independently to produce the effects observed in the data, which suggests a depth-varying Poisson's ratio.